Thesis for Master's Degree

2007

Estimation of the Significant Wave Height from Images of X-Band Nautical Radar System

JIN RONG

Department of Spatial Design and Engineering

Handong Global University

Thesis for Master's Degree

2007

Estimation of the Significant Wave Height from Images of X-Band Nautical Radar System

JIN RONG

Department of Spatial Design and Engineering

Handong Global University

SD JIN RONG
20533005 Estimation of the Significant Wave Height from Images of X-Band Nautical Radar System.
Department of Spatial Design and Engineering , 2007
Advisor : Prof. Kyungmo Ahn.

ABSTRACT

Nowadays, it has been found that the radar images of ocean surface provide reliable information about the spatial behavior of wave fields. Accordingly it is possible to analyze these radar-image sequences regarding the retrieval of directionally unambiguous two-dimensional (2-D) image spectra the mean near-surface current vector, the mean water depth, the significant wave height, and the mean wind speed for the whole measurement area. However, the radar system is only able to determine quantities describing the intensities of the back-scattered electro-magnetic waves form the sea state and wind properties of an area. For estimating the significant wave height an additional calibration procedure is necessary.

In this work, the measurement of ocean waves and surface currents with a nautical radar based on the spatial and temporal structure analysis of radar images of the sea surface is studied, which mainly consists of methods for measuring sea

surface states, X-band radar system, inversion of marine radar images and estimation of significant wave height.

For estimating sea surface elevation maps from sea clutter images acquired by marine radar, an inversion method was used. This method represents an extension of an existing technique to estimate wave spectra from temporal sequences of marine radar images. It is based on the linear wave theory and assumes the wave field homogeneous in space and stationary in time. To obtain additional information about the main imaging mechanisms responsible of the radar imagery, various numerical simulations of swell and wind sea were carried out. For each sea state simulation, the respective radar image was determined assuming shadowing only and shadowing plus tilt modulation.

In order to obtain the significant wave height from sequences of nautical radar images, software was developed. This method is based on a technique developed for the determination of significant wave height information from synthetic aperture radar imagery. The calibration was performed with a set of 100 signal to noise ratio SNR versus the significant wave height Hs. The parameters of the calibration were calculated by least-square fit of the estimations. After the calibration period, the real values of the ocean wave spectra and the wave parameters that characterize the sea state can be estimated.

Contents

List of Tables

List of Figures

I. INRTODUCTION

Real-time information about the sea state, such as wave height, direction and period, is crucial for coastal protection, as well as off-shore operation management (e.g. oil platforms or ships). In the last 30years, routine sea state measurements have been carried out using many different measuring devices such as moored buoys and pressure gages etc[1]. Although such devices provide reliable measurements, they are easily subject to damage and loss. Therefore considerable interest has been shown lately in the use of remote sensing techniques to measure waves and surface currents.

In recent years, it has been demonstrated that radar images of the ocean surface provide reliable information about the spatial behavior of wave fields [*2*]. A Wave Monitoring System (WaMoS) has been developed at GKSS Research Center, Geestacht, Germany, which is in operational use [3-4]. The system utilizes a commeicial nautical X-band radar for providing time series of radar backscatter images from the ocean surface. The radar technique thereby allows measurement under most severe weather conditions. With the pre-existing installations of nautical radar systems at all marine structures, harbors, platforms and ships the measurements can be done in a very cost-efficient way.

Nowadays, it is possible to analyze these radar-image sequences regarding the retrieval of directionally unambiguous two-dimensional (2-D) image spectra *Z*, a mean near-surface current vector [5], the mean water depth [6], the significant wave height, and the mean wind speed for the whole measurement area [7]. The WaMoS system is therefore only able to determine quantities describing the mean sea state in terms of image intensities and wind properties of an area. For estimating the significant wave height an additional calibration procedure, with a buoy for example, is necessary.

In contrast to wave parameter such as peak wave period, peak wave direction or peak wave length, which can be determined directly from the radar images, the significant wave can not determined directly and hence needs a calibration. The reason for this is due to the non-linearity of the imaging mechanism of ocean waves in radar images. In 1982, Aplers and Hasselmann developed a method to derive the significant wave height (Hs) from synthetic aperture radar (SAR) imagery obtained by ERS-1 over the ocean. The basic idea of this method is that Hs is assumed to be linearly correlated with the root square of the signal-to-noise ratio (SNR) of the radar image. The successful use of this method for the determination of the significant wave height from nautical radar images has been shown for various installations [8-10].

According to Alpers and Hasselmann(1982) the measured signal-to-noise ratio （SNR） is linearly correlated with the significant wave height (Hs) of an independent wave sensor:

$$H_s \approx A + B\sqrt{SNR}, \tag{0.1}$$

where A and B are calibration constants which depend on the radar installations. These calibration constants are determined within a calibration period by means of a least squares method:

$$\sum_{i=1}^{N}(H_s(i) - (A + B\sqrt{SNR(i)}))^2 = Min, \tag{0.2}$$

where i is the number of data samples.

The SNR proposed by Alpers and Hasselmann [11] relates the SAR image spectrum with the sum of the clutter and thermal noise spectra. In contrast to this WaMos II relates the spectral energy related to the wave spectrum (SIG) with the remaining signal which is defined as background noise (BGN):

$$SNR = \frac{SIG}{BGN}, \tag{0.3}$$

Where SIG is determined as the sum of the wave spectrum $(E^{(2)}(\vec{k}))$:

$$SIG = \sum_{i=1}^{N_x} (\sum_{j=1}^{N_y} (E^{(2)} \Delta k_x(j)) \Delta k_y(i)) \tag{0.4}$$

BGN is

$$BGN = \sum_{i_x=1}^{N_{kx}} \sum_{j_y=1}^{N_{ky}} \sum_{i_f=1}^{N_{kf}} F^{(3)}(i_x, i_y, i_f) \Delta f(i_f) \Delta k_y(i_x) \Delta k_x(i_y) - \sum_{i_x=1}^{N_{kx}} \sum_{j_y=1}^{N_{ky}} F^{(2)}(i_x, i_y) \Delta k_y(i_x) \Delta k_x(i_y) \tag{0.5}$$

where $F^{(3)}$ represents the 3-D image spectrum

$F^{(2)}$ represents the 2-D image spectrum

N_{kx}, N_{ky} and N_{kf} is the extension of the spectra

Δk_x, Δk_y are wave number resolutions

Δf is frequency resolution.

II. OVERVIEW

2.1 Methods for measuring ocean surface state

Ocean waves which are typically consist of wave periods between 1 and 30 seconds, are usually generated from wind or geologic effects. Growth of waves depends on the fetch and duration of the wind. Waves smaller than 1 second of period are known as ripples for which the restoring force is dominated by surface tension. Generally waves are measured for a period of 20 minutes, with an interred of one to three hours. The analysis of the 20 minute record yields short term statistics with significant wave height, zero crossing period, etc. An analysis of significant wave height, zero crosssing period, etc., over a period of 1–5 years yields long term wave statistics. The highest significant wave height that will occur once in 50 or 100 years is known as extreme waves with specifred return period.

The directional spectrum desaibes the distribution of wave energy density as a function of frequency and direction. A cross-section of the directional spectrum surface for a given frequency, which is a curve depicting the wave energy density as a function of direction is also referred to as the directional spectrum. Essentially the directional spectrum is a representation of the 2- dimensional wave number

spectrum obtained using the dispersion relation for surface waves. The directional spectrum gives a more complete description of the waves occurred at a particular place and time than other representations such as significant wave height and the predominant wave height and direction.

The earliest and the most enduring application of the directional spectrum was in the field of wave forecasting and hindcasting by Pierson et al. [1955], the WAM model of Hasselmann et al. [1988] being its present day analogue. In another case Komar and Inman [1970] have used directional spectra for the study of littoral transport. Directional spectra have been used by for studying the diffraction of wind waves. Directional spectra are also useful for the design and analysis of moorings, offshore towers and piles. For the analysis of vibration and three dimensional analyses of structures with torsional loads, directional spectrum is an input function. Directional spectra are necessary for the study of growth and decay of waves and to acertain the frequency and directional spread of energy density by processes such as resonant interactions. Occurrence of “freak” waves which have been responsible for the destruction of breakwaters in Iceland, Norway and France is thought to be linked with the wave directional spectrum of ocean waves

The three main methods for measuring the wave directional spectrum are through (i) arrays, (ii) buoys and (iii) radar. Arrays and buoys directly measure the

wave directional spectrum, while radar measures it through remote sensing using radio or microwaves. In array type of measurement just one parameter wave elevation is measured at several points in a linear or polygonal array. In buoy type of measurements several different parameters are measured at essentially the same point. In radar type of measurements, the backscatter from Bragg resonant surface waves is measured. It was Crombie [1955] who identified Bragg scattering as the mechanism for imaging “sea-clutter” (ocean waves) from radar echo from sea at High Frequency (dekameter waves). Figure [1-3] shows typical of buoy and radar system.

Fig.1 Buoy

Fig. 2 Radar antenna

Fig. 3 Radar hardware and software system

The wave directional spectrum can also be measured using optical methods including stereophotogrammetry which has been done in the Stereo Wave Observation Project reported by Cote et al. [1960] and Chase et al. [1957], who used two simultaneously taken photographs of the sea surface. Uberoi [1964] used an optical analogue method to determine the wave directional spectra of 2-dimensional functions from single photographs. Stilwell and Pilon [1974] using the concept of continuous skylight luminance function obtained wave directional spectra from single photographs of the sea surface using optical 2-dimensional Fourier Transform technique, utilizing auxiliary data of altitude and azimuth, the method being a generalization of the sun glitter method of Cox and Munk [1954] and Cox [19], which provided statistics of surface slopes but could not determine the wave directional spectrum.

2.2 The operational wave monitoring system

2.2.1 The nautical radar

Nautical radars are usually utilized for detecting targets on the ocean surface. In the open sea the radar systems normally operate at 3.0-3.1 GHz (S-band) with a far range coverage and a coarse radial resolution. In coastal areas a frequency of 9.33-9.5 GHz (X-band) is used, aiming at a high radial resolution with a smaller covered

area. Because of the higher resolution, X-band devices are utilized for sea state measurements. The polarization is usually HH in transmit and receive, because for navigation purposes the radar backscatter from the sea surface is smaller than with VV polarization [12].

The nautical radar is a mono static system. The same antenna is alternately sending and receiving. The antenna is directional and radiates electromagnetic energy in patterns of lobes that extend outward from the antenna in one direction for a given antenna position. The radiation pattern also contains minor lobes, but these lobes are weak and normally have little effect on the main radiation pattern. Further, the system is pulse limited for determining the radial position of the backscattered signal by measuring the signal run time. The radial resolution ρr is limited by the pulse duration τ. Under grazing incidence the radial resolution is given with $\rho r = c\tau/2$, where c is the speed of light.

The sending signal of a nautical radar is coherent. It consists of both amplitude and phase-information. From the backscattered signal only the modulus of the complex signal is recorded. The phase information is not considered. The intensity of the radar backscatter from the ocean surface decreases from near range to far range with r^{-2}. The area of a resolution cell increases proportional to the distance from the radar, resulting in a received power proportional to r^{-3}. For compensation

of this r^{-3} decrease, a time-dependent amplifier is operated. Additionally, at the video output of the radar system, a signal-dependent logarithmic amplifier is operated to get a larger dynamic range. A normed radar cross section of each resolution cell is not measured by a nautical radar. The measurements are done with a non-calibrated radar with incoherent receive.

2.2.2 WaMoS II SYSTEM

The Wave Monitoring System WaMoS II, based on a commercially available nautical X-Band radar, was developed for real time measurements of directional ocean waves spectra.

WaMoS II permits objective measurements of the sea state. By analysing the spatial and temporal evolution of the radar backscatter from the sea surface this system allows to obtain unambiguous directional wave information. The measurement is based on the backscatter of microwaves from the sea surface, which is known as 'sea clutter' on common nautical radar units. There from all other relevant sea state parameters are derived in real time, such as significant wave height, wave periods, wave lengths and directions. Many comparisons between in situ wave sensors and WaMoS II data show the capabilities of navigational radars in providing absolute wave heights, wave periods and directions with a certain

degree of accuracy. Those data comparisons showed that WaMoS II claims to reach about the same accuracy as a conventional wave rider buoy.

The system is especially designed for the operation from fixed and moving platforms, and on board all types of ocean going vessels. The overall advantage of WaMoS II is, the continuous availability of wave data in very rough sea conditions even under harsh weather conditions and during night with limited visibility.

WaMoS II is a hardware and software “data capture system” for wave and current monitoring purposes consisting of an A/D converter, a PC, and a processing software connected to a marine X-Band radar (9.41 GHz), which is shown in Figure 4.

The minimum radar requirements for wave analysis purposes are:

(1) A minimum antenna rotation speed of 24 rpm (antenna rotation time: RPT<2.5s),

(2) A maximum radar pulse length of 80 nsec,

(3) A minimum antenna length of 2.44m.

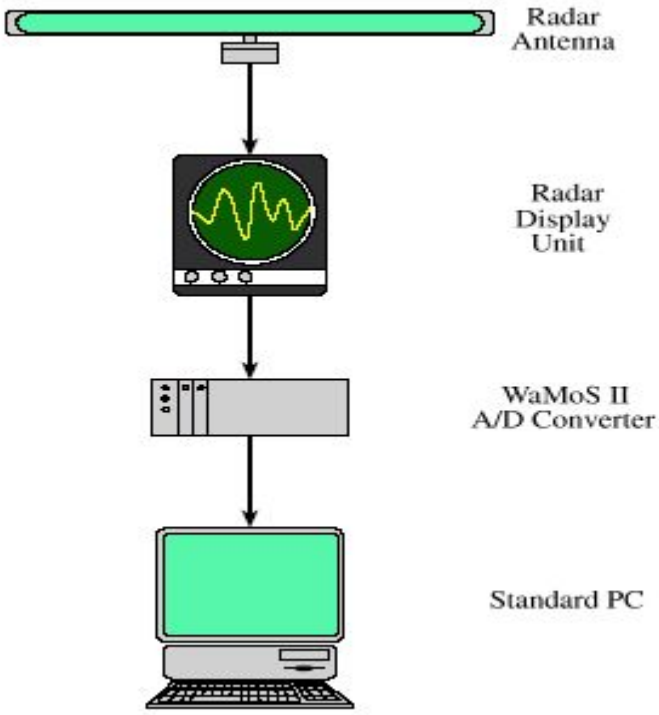

Fig. 4 Schematic drawing of a WaMoS II measuring device

In connection with a nowadays standard radar (r.p.l.=43rpm, RPT=1.4s, antenna length = 2.44m) WAMOS II obtains radar images with a range resolution of 8.5 m and an angular resolution of 0.09º for every radar rotation. For the standard V analysis a sequence of 32radar images is used, so that waves in frequency range between 0.025 Hz and 0.29Hz can be detected. This frequency range corresponds to wave periods 3.5 s and 55.5 s. for wave measurements the radar system must be operated in the near range. Typical WAMOS II operating ranges are between 0.1 km to 5km, depending mainly on the wind speed and the

installation height. The minimum wind speed required for operational measurements is around 3 ms^{-1} [13].

Fig. 6 mobile radar system used in this work

Table.1 Parameters of the X-Band radar system

Frequency	X-Band 9410+30MHz	
Peak Power out put	X-Band 25kW nominal	
Magnetron Life	10,000 Hours typical	
Pulse length and PRF		Range Scale (Nautical Miles)
Short(S)	X-Band 0.07 μ s(0.045-0.085) 1500+40, or 3000 pps+80	0.125 0.25 0.5 0.75 1.5
Medium (M)	0.25 μ s (0.20-0.30) 750 pps+20 or 1500+40	3.0 6.0 12 24 48 96
Long (L)	1.0 μ s (0.85-1.0) 750pps +20	48 96
Synch. output	3×75 Ohm outputs (Downmast) 1×75 Ohm outputs (upmast) not less than +12V amplitude	
Receiver (used for all transceivers)		
Type Transfer Characteristics I.F. Video Output	Logarithmic Receiver Nominal 60MHz 3× 75 Ohm outputs (Downmast) 1× 75 Ohm outputs (Upmast) 5.5 peak amplitude	

III. INVERSION OF MARINE RADAR IMAGES FOR SURFACE WAVE ANALYSIS

3.1 Introduction

It is known that under various conditions signatures of the sea surface are visible in the near range (<3nmi) of marine radar images. These signatures are known as sea clutter because they are undesirable for navigation purposes and generally suppressed by filter algorithms. Sea clutter is mainly due to the backscatter through Bragg resonance with ocean waves of wavelengths similar to those of the transmitted electromagnetic waves. The longer waves become visible in the radar images because they modulate the sea clutter signals. The modulation is a nonlinear process mainly affected by three effects: hydrodynamic modulation (HM), tilt modulation (TM), and shadowing (SH), where HM describes the modulation of the energy of the ripples by the interaction with the longer waves, TM the modulation due to the changes of the effective incidence angle along the long wave slope, and SH the partially shadowing of the sea surface by higher waves [14-16]. Hence the sea clutter radar image intensities do not map on a one-to-one scale the ocean surface elevation. Since marine radar systems give the opportunity to scan the sea surface with high temporal and spatial resolution, it allows monitoring of the sea state [17-20]. The objective of chapter 3 is to demonstrate the ability to invert sea clutter images into sea surface elevation maps,

which are estimations of the waves images by the radar. This inversion scheme allows the investigation of single wave properties, such as, for example, wave height and crest steepness. This is especially of importance for the investigation of rogue waves (singular appearing wave phenomenon that cannot be described by common wave statistics).

3.2 Simulation of wave images

3.2.1 Theoretical wave elevation simulation

To derive sea state parameters from sea clutter time series g(r, t) the concept of sea state is taken into account, which is based on linear wave theory and assumes spatial homogeneity and temporal stationary of the wave field. Under these assumptions, sea states are described as Gaussian zero-mean random processes varying in space r=(x, y) and time t, with vertical wave elevations over the mean sea level η having the following spectral representation:

$$\eta(r,t) = \sum_{m=1}^{N_x} \sum_{n=1}^{N_y} A_{mn} \cos[k_{mn} \cdot r - \varpi(k_{mn})t - \vartheta_{mn}] \quad \textbf{(3.1)}$$

Where k = (k_x , k_y) is the wavenumber vector,

ω is the angular frequency,

ϑ_{mn} are uniformly distributed random phases on the interval [- π , π].

Assuming the linear wave theory is valid, ocean surface waves are dispersive with a dispersion relation given by

$$\omega = \varpi(k) = \sqrt{gk \tanh(kh)} + k \cdot U \qquad \textbf{(3.2)}$$

Where $k = \|k\|$

g is the acceleration due to gravity,

h is the water depth,

$U = (U_x, U_y)$ is the surface current.

3.2.2 Numerical Simulation of Sea Clutter Images

To derive some of the marine radar imaging properties a numerical stochastic simulation model of the sea surface has been used. Assuming the linear wave model,

and different sea state conditions were considered by applying different theoretical frequency spectra: Wallops for swell and JONSWAP for wind sea cases.

$$S(f) = \frac{0.0624}{0.23 + 0.033\gamma - 0.185(1.9+\gamma)^{-1}} H_s^2 f^{-5} f_p^{-4} \exp(-1.25(f/f_p)^{-4}) \gamma^{\exp(\frac{[f/f_p - 1]^2}{2\delta^2})}$$

(3.3)

$$\text{where, } \sigma = \begin{cases} 0.07 & f \le f_p \\ 0.09 & f > f_p \end{cases}$$

For the directional spreading function $G(f,\theta)$, a squared cosine distribution was used:

$$G(f;\theta) = \frac{2^{2s-1}}{\pi} \frac{\Gamma^2(s+1)}{\Gamma(2s+1)} \cos^{2s}\left(\frac{|\theta - \bar{\theta}|}{2}\right) \qquad (3.4)$$

where Γ is the gamma function, and the mean wave direction is given by $\bar{\theta}$, here assume $\bar{\theta}$ is 0. The parameter s leads the angular spreading; s is a function of the wave frequency $f = \omega / 2\pi$. The parameterization for the function $S(f)$ given by [21] has been used,

$$s = s_{max} \left(\frac{f}{f_p} \right)^{\mu} \tag{3.5}$$

where μ has two different values depending on the wave frequency;

$$\mu = \begin{cases} 5.0 & f \le f_p \\ -2.5 & f > f_p \end{cases} \tag{3.6}$$

Frequency mapping can be done using Goda's formula

$$f_i = \frac{1.007}{T_s} \left(\ln \left(\frac{2M}{2i-1} \right) \right)^{-0.25} \tag{3.7}$$

where M is number of frequency components.

For our simulation, the significant wave height equals to 4m has been used for swell and wind sea cases. In addition, the angular spreading for the peak frequency was obtained taking into account empirical values of s_{max} determined for swell and wind sea. The used values of s_{max} are given in Table 2.

Table 2. Angular spreading $s_{\max}$ for the numerical sea state simulations of swell and wind sea.

Sea state	Peak frequencies [Hz]	$s_{\max}$
Swell	0.08, 0.09	75
	0.1	25
Wind sea	0.1, 0.12, 0.14	10

The final result is shown in figure 7, where the light areas correspond to wave crest and the black areas to wave troughs. In Fig 7, sea surface elevation η is grayscaled.

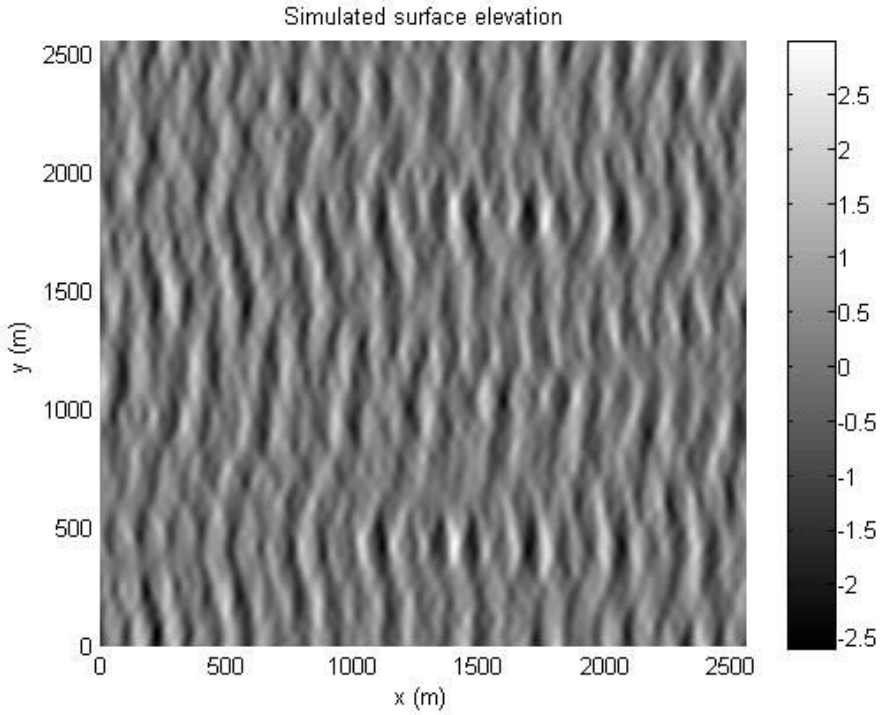

Fig 7-1 Number of frequency components =3 Number of direction components=50, $s_{\max}$ =75.

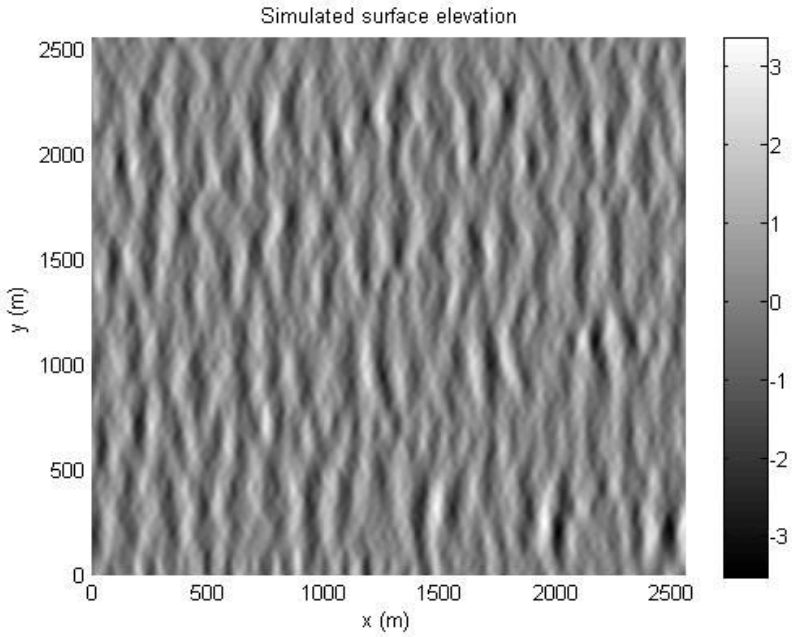

Fig 7-2 Number of frequency components =5, Number of direction components=50, $S_{\max}$ =75.

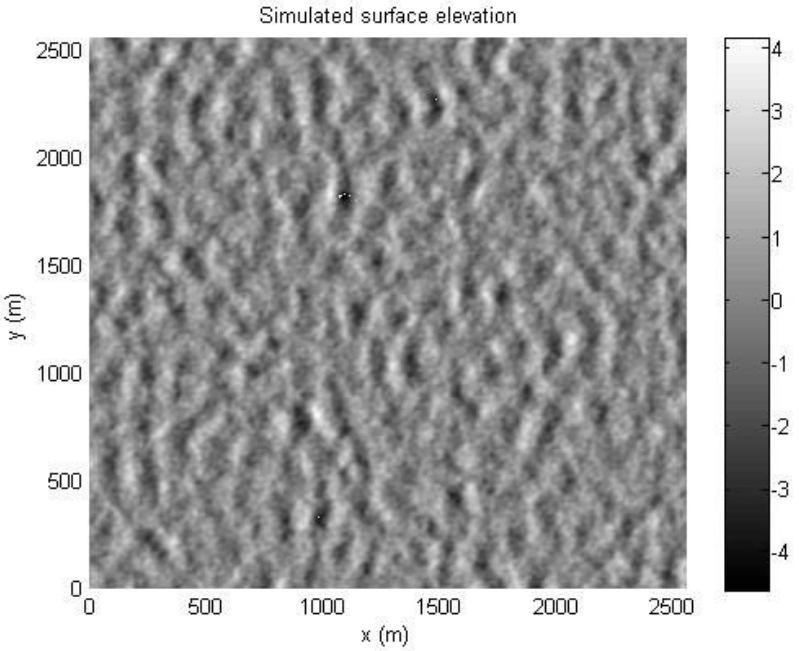

Fig 7-3 Number of frequency components =30, Number of direction components=50, $S_{\max}$ =10.

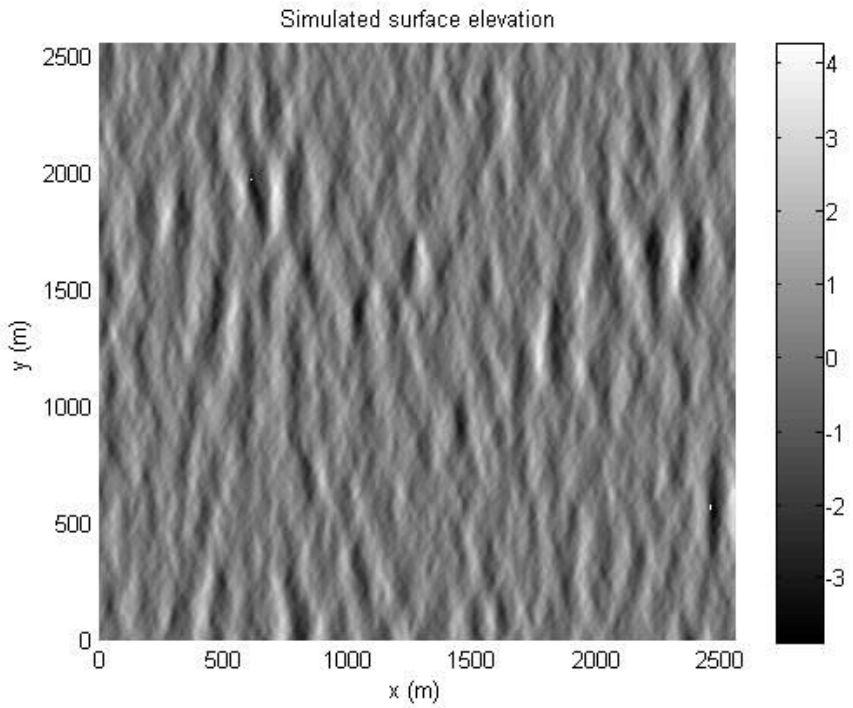

Fig 7-4 Number of frequency components =30, Number of direction components=50, $S_{\max}$ =75.

3.3 Shadowing Modulation

For far-range and horizontal polarization, geometrical optics approximation is assumed [22]. Hence, for grazing incidence the local incidence angle on an illuminated facet (which is related to the radar resolution cell located at point r and at time t) is

$$\theta_0(r,t) = \tan^{-1}\{R(r)/[\Lambda - \eta(r,t)]\} \qquad (3.8)$$

where $R(r)$ is the range and Λ is the antenna height over the sea level. See fig 8.

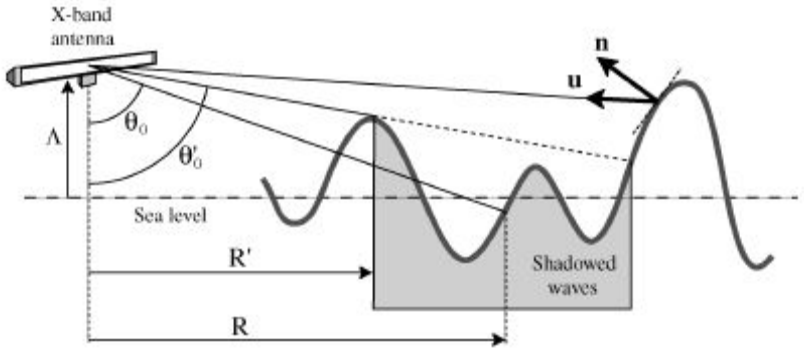

Fig. 8. Scheme showing the geometrical method to simulate wave shadowing. A wave facet, at range R, is shadowed to the antenna if there is another facet in the same azimuthal angle with $R' < R$, for which, $\theta_0' < \theta_0$. In addition, the figure shows the mechanism to simulate tilt modulation at grazing incidence by using the scalar product of the 3D unit wave surface exterior vector n and the 3D unit vector from the sea surface to the antenna u.

The facet will be shadowed to the antenna if another facet [located at the point r', with $R' = R(r') < R(r)$, at the same azimuthal angle than r] has a local incidence angle

$$\theta_0' = \theta_0(r',t) >= \theta_0(r,t) \qquad (3.9)$$

The simulated shadowed image is given by Nieto Borge 1997

$$\sigma_{sh}(r,t) = \begin{cases} \sigma(\mathrm{r,t}), & \text{if no shadowing occurs} \\ 0 \quad , & \text{otherwise} \end{cases} \tag{3.10}$$

where $\sigma(r,t)$ is obtained by rescaling the values of $\eta(r,t)$ into 256 gray levels. Note that $\sigma(r,t)$ is only a first-order approximation of the digital radar output, as the radar intensity is not proportional to the wave height. Nevertheless, this is an adequate assumption for our investigation, as hydrodynamic and tilt modulation have a minor impact on the imaging mechanism compared to shadowing at grazing incidence [23]. See figure 9 shows the corresponding shadowing mask for an antenna at 1250m distance and 30m above the mean level. Here black (white) indicates shadowed (illuminated) areas.

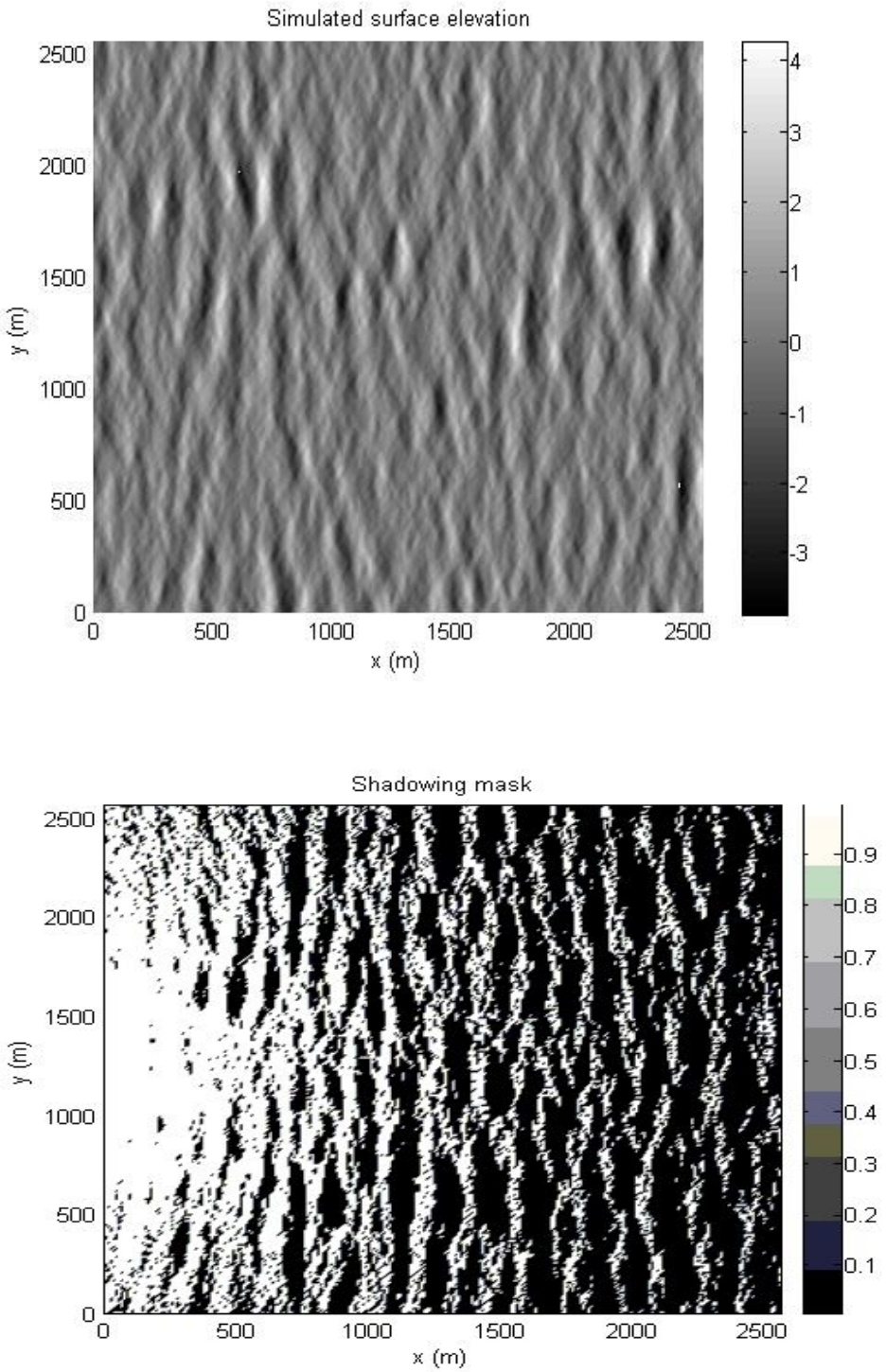

Fig 9 Corresponding shadowing mask assuming an antenna 30m above sea level,

3.4 Tilt Modulation

At grazing incidence, the tilt modulation depends on each facet orientation and facet range. This effect is simulated by using the scalar product between the 3-D unit exterior normal vector n(r, t) to the simulated surface, and the 3-D unit vector from the facet to the antenna, u(r, t) (see Fig.3). Analytically, the normal exterior vector is given by

$$n = (\rho_x \times \rho_y) \left\| \rho_x \times \rho_y \right\| \qquad (3.11)$$

Where $\rho_x = (1, 0, \frac{\partial \eta}{\partial x})$ and $\rho_y = (1, 0, \frac{\partial \eta}{\partial x})$ are the 3D tangent vectors on the surface $\eta(r,t)$.

Hence, the tilt simulated image is given by the factor $\tau(r,t) = n(r,t) \cdot u(r,t)$

$$\sigma_{tilt}(r,t) = \begin{cases} \tau(\mathrm{r,t}), \text{ if } \tau(\mathrm{r,t}) > 0 \text{ and } \sigma_{\mathrm{sh}}(r,t) \neq 0 \\ 0\ , \qquad \text{otherwise} \end{cases} \qquad (3.12)$$

Finally, the $\sigma_{tilt}(r,t)$ values are coded with 256 gray levels. Figure 10 illustrates the results of a sea state simulation for a $2560\mathrm{m} \times 2560\mathrm{m}$ area. The

simulation was carried out for a Jonswap spectrum with Hs=4m and a peak frequency f_p =0.1 Hz.

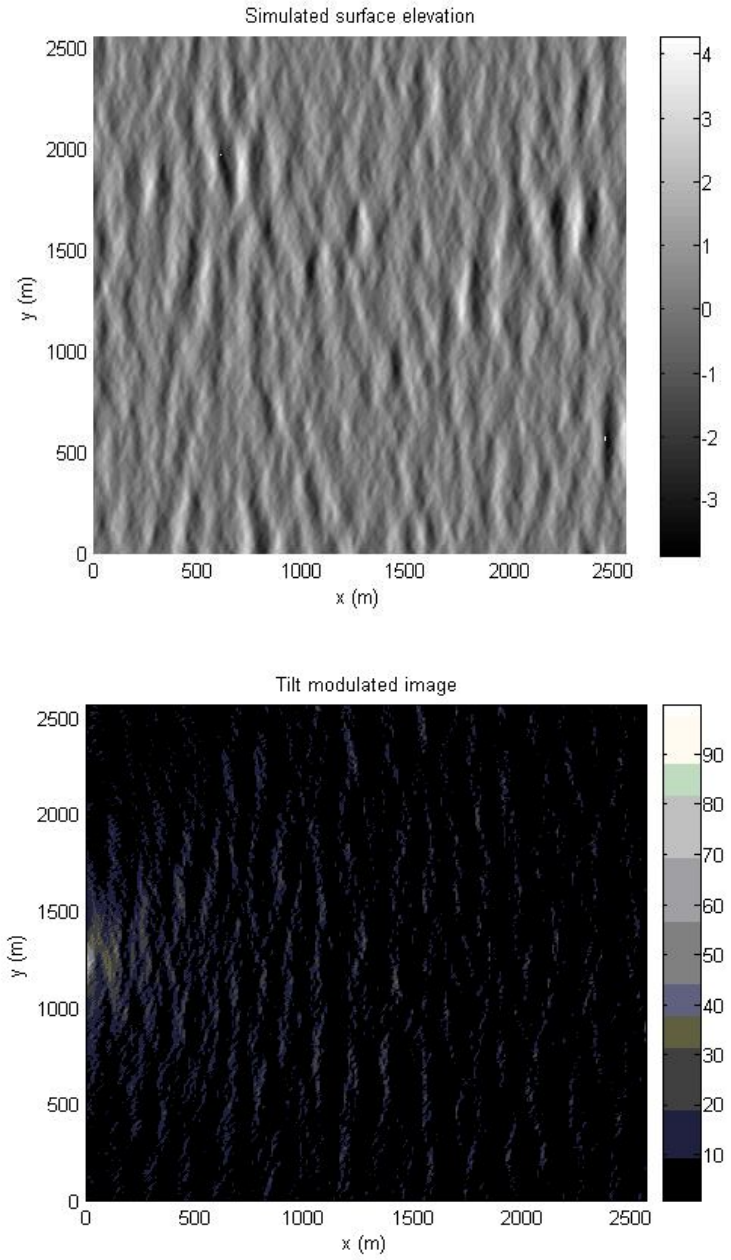

Fig 10 Simulated sea clutter image where additional tilt modulation has been applied

IV. Estimation of Significant Wave Height

4.1 Introduction

With growing need of sea state information, in the last decades different sensors have been developed. Special interest has been shown lately in the use of remote sensing techniques to measure waves and surface currents. One technique to remotely measure the sea state is based on a nautical X-Band radar used generally for traffic control and navigation purposes. The fundamental interaction between the radar and the sea surface is assumed to be Bragg scattering, hence the small ripples are responsible for the radar return [24]. The longer surface gravity waves become visible in the radar images by: hydrodynamic modulation, tilt modulation and shadowing [25-27]. In order to derive wave information from radar images the temporal and spatial evolution of the radar backscatter information of the sea surface is analyzed by means of a discrete Fourier analysis, where spatial and temporal homogeneity within the observed area is assumed [28]. Various comparisons of different sea state parameter inferred from nautical radar and buoy measurements, have been proved the reliability of this technique in order to derive energy and unambiguous directional distribution of ocean waves and the surface current [29-30].

In contrast to in-situ sensors, which are measuring the temporal evolution of the surface elevation at a given location, absolute values of the wave heights cannot be determined directly from radar images. In 1982 Alpers and Hasselmann developed a method to derive the significant wave height from synthetic aperture radar (SAR) imagery obtained by ERS-1 over the ocean. The basic idea of this method is that the significant wave height is assumed to be linearly correlated to the root square of the signal-to-noise ratio of the radar image. The general possibility to use this method also for the determination of the significant wave height from nautical radar images has been shown for various installations

The significant wave height H_s is the most important quantity used describing a sea state. H_s is used for evaluating the impact of waves and breakers onto watercraft, breakwaters or harbor constructions, in the open sea and coastal zones. It is usually determined directly from a wave record in a number of ways.

So in this chapter, we will deal with a method to obtain the significant wave height from sequences of nautical radar images. The method is based on a technique developed for the determination of significant wave height information from synthetic aperture radar imagery.

4.2 Procedure

To measure sea states using marine radars, it is necessary to have a minimum amount of wind, typically higher than 3 m/s so as to produce ripples on the sea surface. These ripples interact with the electromagnetic fields emitted by the radar transmitter. Hence, what the radar receiver captures is the modulation of the backscatter pattern with the longer waves (wind sea or swell). It is important to remark, that the final image in the radar screen is not a map of the wave field, but an image containing information about how the sea surface backscatters the electromagnetic fields. So, phenomena such as the wind speed, the wave tilts, and the wave heights affect the data.

To extract wave information from the radar imaging it is necessary to apply an inversion analysis technique in order to filter out the spectral components of the radar image spectrum and to estimate the wave spectral density, which leads to all sea state parameters. Taking into account the actual microprocessor technology, the required computer time to process common marine radar data sets is about 2 minutes. Hence, nautical radars are suitable to be used as a real time sensor for sea state monitoring. As mentioned above, a typical marine radar measurement is composed of a temporal sequence of sea clutter images $I(x, y, t)$. This data set contains information about several phenomena, such as the wave field spatial and

temporal dependence, the wind speed, etc. The method of analysis takes into account the theoretical dependence of the spatial and the temporal evolution of linear waves. This method is composed of several steps, which are described below.

1. Image Transformation

For the data analysis a subimage of 1 km x 2 km is extracted out of the full polar radar image and transformed into Cartesian coordinates.

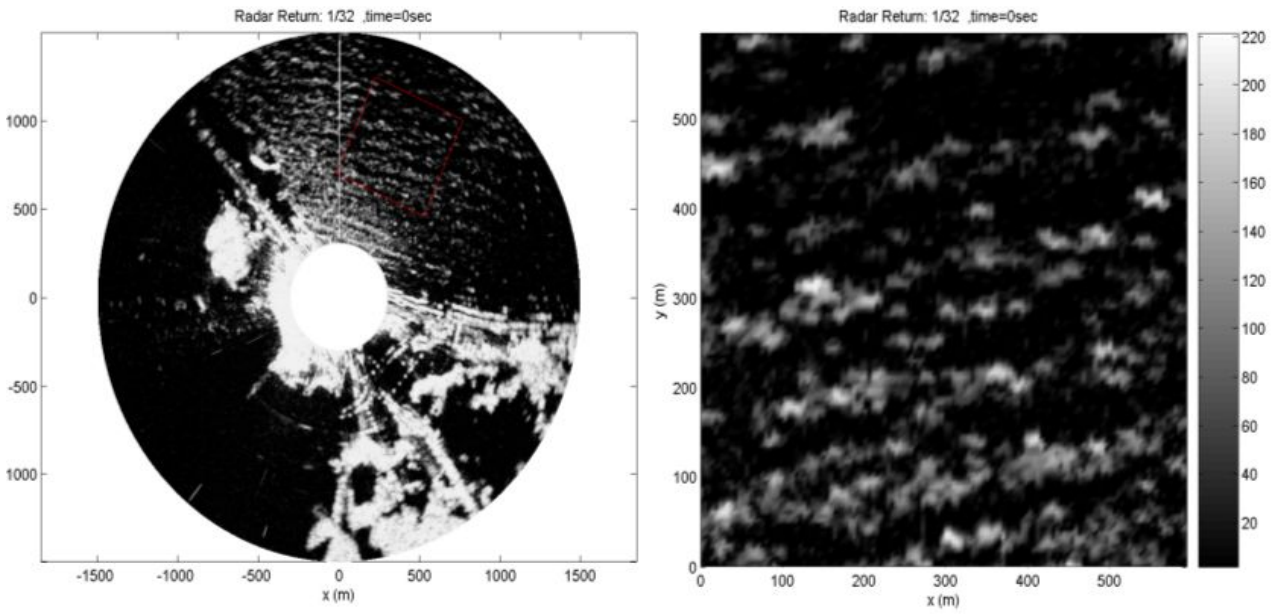

Fig 11 Transform polar radar image into Cartesian coordinates.

2. Discrete Fourier Transformation

The sequence of radar subimages is transformed into a 3-D image spectrum by using a discrete Fourier Transform.

3. Surface current determination

The surface current is obtained by minimizing the distance between the position where spectral energy is located in the measured 3-D image spectrum and its theoretical position given by the dispersions relation for linear surface gravity waves [31].

4. Filtering the 3-D image spectrum

The energy associated with the ocean waves is separated from the background noise by applying the dispersion relation as a pass-band filter.

5. Determination of the 2-D image spectrum

Integration of the 3-D image spectrum over the positive frequency domain in order to obtain a non-ambiguous directional 2-D image spectrum [32].

6. Determination of the 2-D wave spectrum

Transformation of the 2-D image spectrum into a 2-D wave spectrum by using a Modulation Transfer Function (MTF)

7. Computation of the directional wave spectrum

Transformation of the 2-D wave spectrum from the wave number space into the frequency direction space.

From the 2-D wave spectrum all important sea state parameters can be derived in real time. Table 3 gives names and symbols of the major sea state parameters and the corresponding ranges and accuracies provided by then standard WaMoS II. Figure 12 gives Scheme of the analysis of sea clutter time series.

Table 3 : Notation, definition, range and accuracy of wave parameters provided by WaMoSII

Name	Symbol	Definition	Range	Accur
2d wave number spectrum	$E^{(2)}(k_x,k_y)$	$E^{(2)}(k_x,k_y) = MTF \cdot F_f^{(2)}(k_x,k_y)$		
2d frequency direction spectrum	$I^{(2)}(f,\theta)$	$\lvert k\rvert \frac{\partial \lvert k\rvert}{\partial \omega} E^{(2)}(k_x,k_y)$	0.025-0.29Hz 0-360^o	

1d frequency spectrum	S(f)	$\int_0^{360^o} E^{(2)}(f,\theta)d\theta$	0.025-0.29Hz	
Significant wave height	Hs	A+B $\sqrt{SNR}$	1m-20m	+/- 10%
Mean period(Mean zero up crossing period)	T_{m02}	$\sqrt{\frac{\int S(f)df}{f^2 S(f)df}}$	3.5-55s	+/- 0.5s
Peak period	T_p	$1/\overline{f}$ $\overline{f} = \hat{f}$ for s$(\hat{f}) > 0.8 \cdot \max(S(f))$	3.5-55s	+/- 0.5s
Mean wave direction	$\theta(f)$	$\arctan(b(f)/a(f))^{-1}$	0-360^o	+/- 2^o
Peak direction	θ_p	$\theta(f)$; $f_p = 1/T_p$	0-360^o	+/- 2^o
Integrated wave spreading	$\theta(f)$	$\theta(f) = \sqrt[4]{2(1-r(f))}$; $r(f) = \sqrt{a^2(f)+b^2(f)}$	0-90^0	
Peak wave length	λ_p	$\omega_p = 2\pi/T_p$; $\lambda_p = 2\pi/\lvert k_p \rvert$	19-600m^3	
1st peak period	T_{p1}	$1/f_1$; $E(f_{p1},\theta_{p1}) =$ $\max(E(f,\theta))$	3.5-55s	+/- 0.5s
1st peak wave length	λ_{p1}	$\omega_{pl} = 2\pi/T_{pl}$; $\lambda_{pl} = 2\pi/\lvert k_{pl} \rvert$	19-600m^3	
1st peak direction	θ_p	$\theta(f_{p1})$	0-360^o	+/- 2^o
2nd peak wave length	λ_{p2}	$\omega_{p2} = 2\pi/T_{p2}$; $\lambda_{pl} = 2\pi/\lvert k_{pl} \rvert$	19-600m^3	
2nd peak period	T_{p2}	$1/f_2$ $\max_2(E(f,\theta)) =$ $E(f_{p2},\theta_{p2})$	3.5-55s	+/- 0.5s
2nd peak direction	θ_p	$\theta(f_{p2})$	0-360^o	+/- 2^o

Surface current velocity	U		0-20ms^{-1}	+/-0.2ms^{-1}
Surface current direction	θ_U		0-360^o	+/-2^o

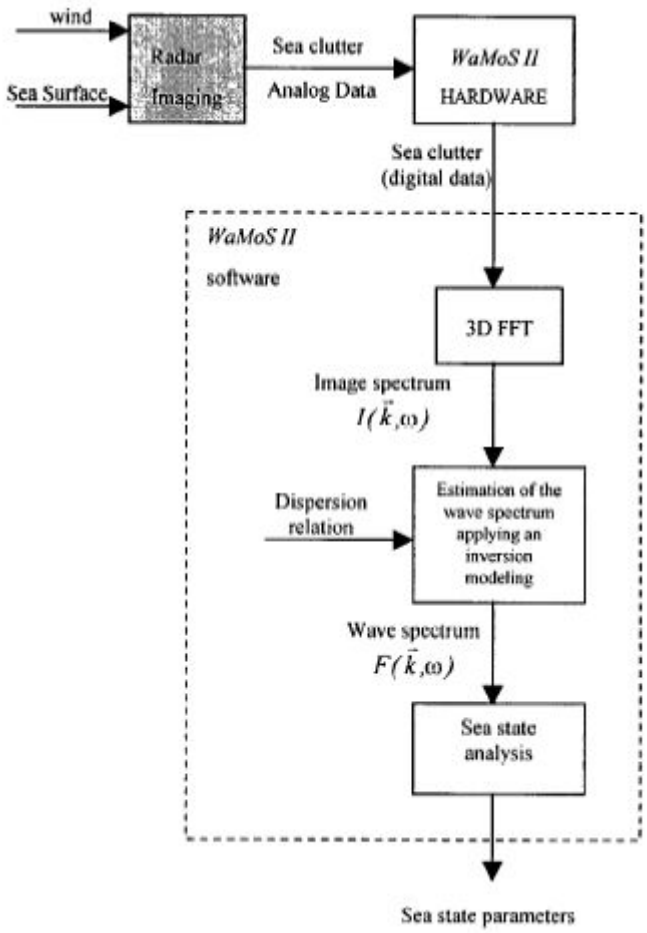

Figure 12 Scheme of the analysis of sea clutter time series

4.3 Detail data processing

4.3.1 Image transformation

Figure 13 shows an example of sea clutter image sampled with the WaMoS II system, at a radar station located in the Sondao beach. Each measurement consists of a temporal sequence of radar images of the sea surface, which is a sea clutter time series. Hence the data contains information about the wave field dependence in space and time. The spatial and temporal sampling resolutions of these radar image time series depend on the technical features of the marine radar used.

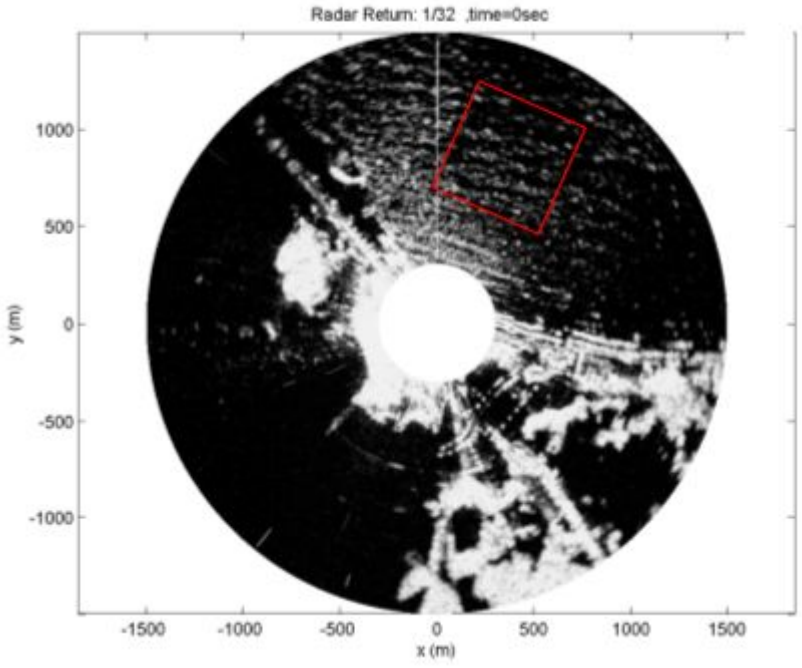

Fig.13 Polar image obtained from WaMos II at Hwayin beach

For image transformation, a subimage of 600 *600 was extracted out of the full polar radar image and transformed into Cartesian coordinates, which is shown in Figure 14.

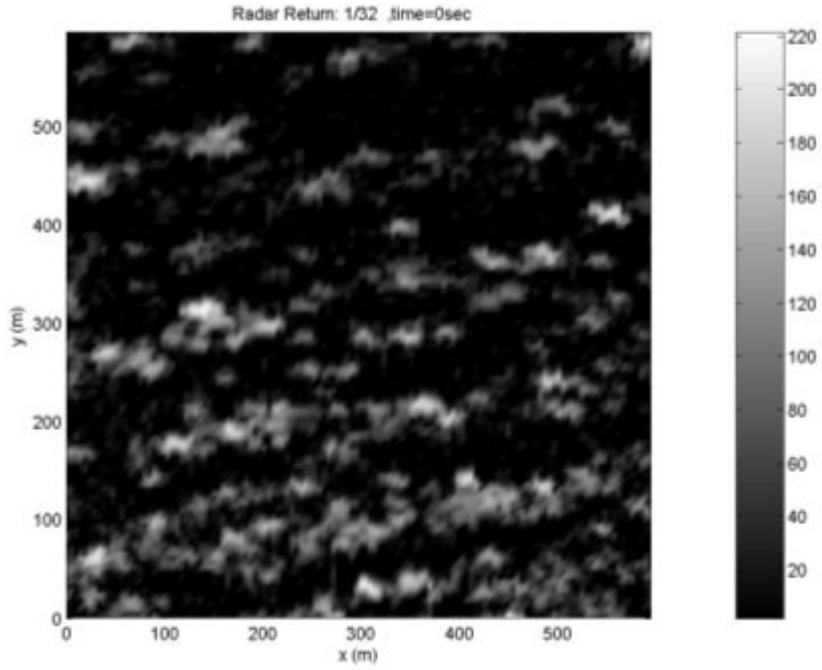

Fig. 14 (a) Cartesian image

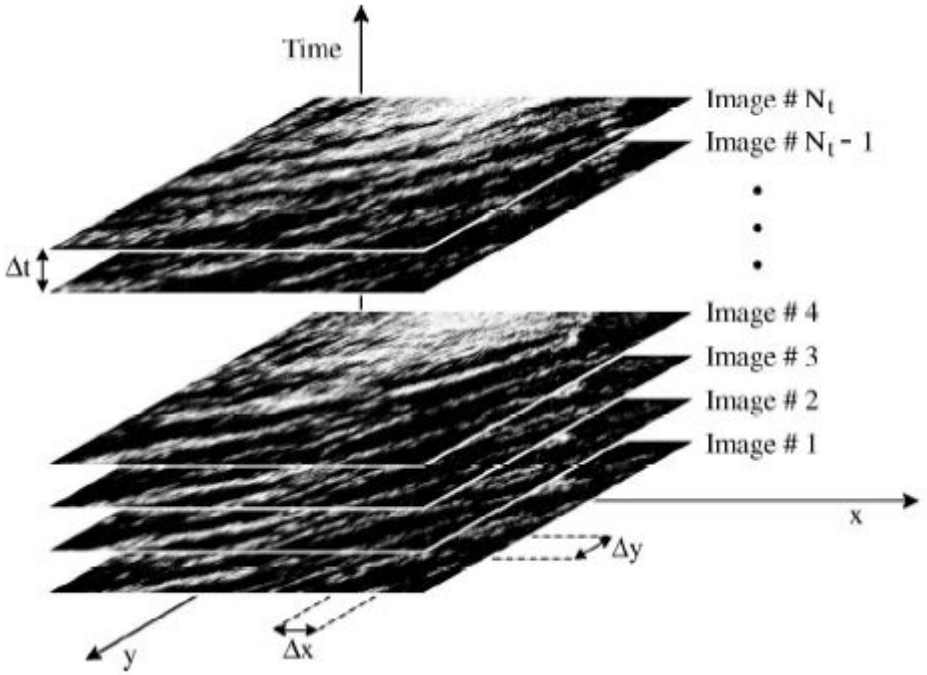

FIG. 14 (b) Temporal sequence of sea clutter images. The grayscale corresponds to the radar backscatter strength. The temporal resolution D*t* is given by the antenna rotation period. The spatial resolutions D*x* and D*y* are dependent on the azimuthal resolution due to the effective aperture of the antenna and on the range resolution due to the radar pulse length[19].

4.3.2 Discrete Fourier Transformation:

The radar image sequence, referring to the radar sub-area $\eta(x,y,t)$ is transformed into the spectral domain by using a Discrete Fourier Transformation :

$$F^{(3)}(k_x,k_y,\omega)=\left|\int_{-k_{xc}}^{k_{xc}}\int_{-k_{yc}}^{k_y c}\int_{-\omega c}^{\omega c}\eta(x,y,t)\exp(i(k_x x+k_y y-\omega t))\,d\omega dk_x dk_y\right| \tag{4.1}$$

Here $F^{(3)}(k_x, k_y, \omega)$ is the three dimensional image spectrum, $\vec{k}$ = (*kx*, *ky*) is the two dimensional wave number vector, and ω is the angular frequency. The Nyquist limits for each spectral variable are given by $k_{xc} = \pi / \Delta x$, $k_{yc} = \pi / \Delta y$, and $\omega_c = \pi / \Delta t$, where Δx and Δy is the spatial resolution of the radar image and Δt corresponds to the temporal resolution of the time series. The resolution for each spectral variable is given by $dk_x = 2\pi / L_x, dk_y = 2\pi / L_{y,} and\ d\omega = 2\pi / T$, where $L_x\ and\ L_y$ are the horizontal extensions of the sub-area η and T is the duration of the measurement and therefore the length of the time series.

4.3.3 Surface current determination

4.3.3.1 Definition

The velocity of encounter $\vec{U}$ is the vector sum of the platform's (i.e., a ship) velocity $\vec{U}_s$ and the near-surface current velocity $\vec{U}_c(z)$, where z is the vertical coordinate. The accuracy of the near-surface current velocity measured by a radar depends on the actual sea state (frequency-shifted by the Doppler effect) since the imaged wave field is the carrier of the velocity information. The Doppler-frequency shift is induced by the near-surface current down to the penetration depth of the waves. The penetration depth for a single wave is approximately half of its

wavelength $h_\lambda = \lambda / 2$ [33] have shown that the component of the velocity of encounter in the direction of the wavenumber vector is a weighted mean current over the upper layer of the ocean. This result has been extended to consider the full current vector[34]

$$\overset{\mathrm{r}}{U}(z) = 2k\int_{-d}^{0} \overset{\mathrm{r}}{U}(z)_c e^{(2kz)} dz \tag{4.2}$$

Where $\overset{\iota}{U}_c(z)$ is the vertical velocity vector profile. This definition is for a single wave.

4.3.3.2 Method of determination of velocity of encounter

The method used to determine the velocity of encounter is based on an adaptation of the dispersion relation of sea-surface gravity waves to the wavenumber components k_x and k_y and frequency ω coordinates of the sea-state signal found in the spectrum $F^{(3)}(k_x, k_y, \omega)$. This adaptation was realized with a least-squares regression method. In the Ω-domain, a curved plane described by the dispersion relation of linear gravity waves is defined

$$\varsigma^2(k) = gk \tanh(kh) \tag{4.3}$$

Where ς intrinsic frequency;

g acceleration due to gravity;

k modulus of the two-dimensional (2-D) wavenumber vector ;

d water depth.

The dispersion relation is valid when the sensor velocity and the near-surface currents are zero.

The so-called *dispersion shell* is illustrated in Fig. 15(a). Imaging of surface waves by nautical radar is nonlinear. The linear part, described by an image transfer function (ITF), results in spectral energy, which is localized on the dispersion shell. The impact of the Doppler term ω_D added to the intrinsic frequency ς is illustrated in Fig. 2(b) and is described as

$$\omega(\vec{k}, \vec{u}_e) = \varsigma + \omega_D \tag{4.4}$$

Where $\omega_D = ku_e \cos(\theta)$ is the frequency of encounter (or the absolute frequency), and θ is the angle between $\vec{k}$ and $\vec{u}_e$. The dependency on the cosine function of ω_D implies that only the component of $\vec{u}_e$ parallel to the wave's travel direction given by the wavenumber vector $\vec{k}$ effects the Doppler-frequency shift.

The Doppler term $\omega_D = ku_e \cos(\theta)$ can be written in Cartesian coordinates as follows:

$$\omega_D = k_x u_x + k_y u_y \tag{4.5}$$

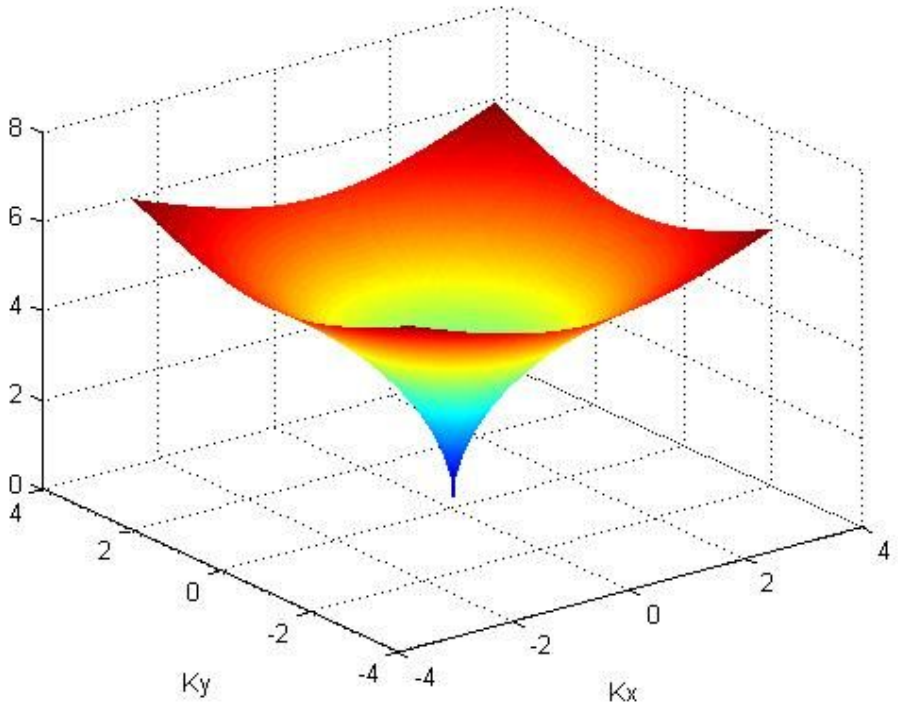

Fig. 15(a) Intrinsic

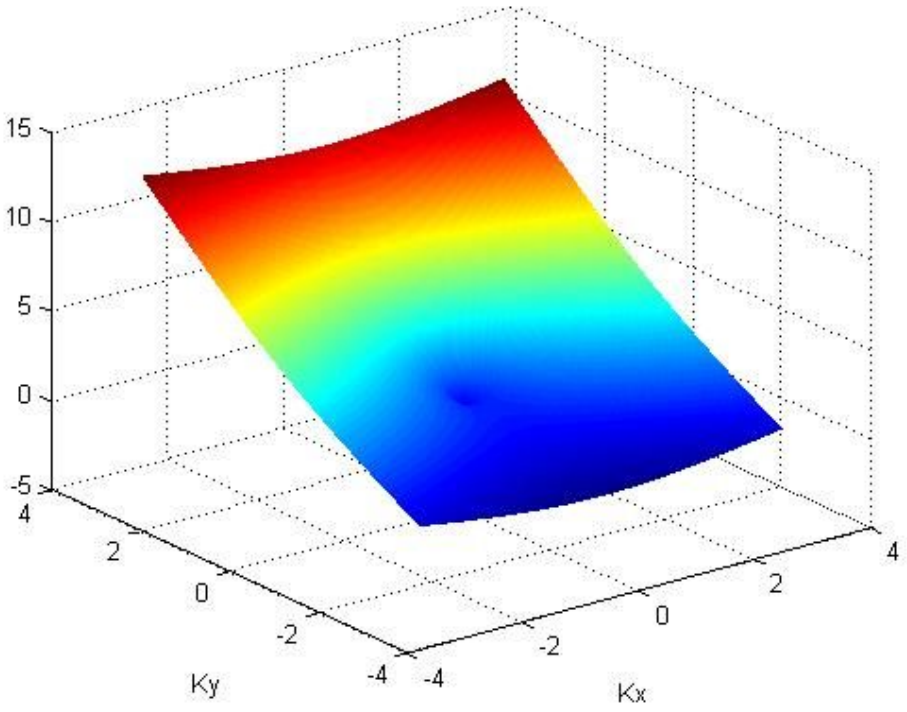

Fig.15 (b) Doppler-shifted dispersion shell in the Ω-domain

The current $\vec{U}$ may be estimated, using a weighted least squares method, by minimizing the function

$$J = \sum_{\omega=0}^{\omega_m} \sum_{k_x=-k_{xN}}^{k_{xN}} \sum_{k_y=-k_{yN}}^{k_{yN}} (\Delta\omega)^2 F(k_x, k_y, \omega) \tag{4.6}$$

where

$$\Delta\omega = \omega - \sqrt{g\left|\vec{k}\right|} - k_x U_x - k_y U_y \tag{4.7}$$

Assuming deep water compared to the wave length, that is

$$\left|\vec{k}\right| d >> 1$$

$F^{(3)}(k_x, k_y, \omega)$ is the 3-D wavenumber/frequency spectrum, and U_x and U_y are the x and y components of $\vec{U}$. The solution with respect to U_x and U_y is

$$\begin{bmatrix} U_x \\ U_y \end{bmatrix} = \begin{bmatrix} \sum E k_x^2 & \sum E k_x k_y \\ \sum E k_x k_y & \sum E k_y^2 \end{bmatrix}^{-1} \begin{bmatrix} \sum E(\omega - \sqrt{g\left|\vec{k}\right|} k_x) \\ \sum E(\omega - \sqrt{g\left|\vec{k}\right|} k_y) \end{bmatrix} \tag{4.8}$$

4.3.4 Filtering the 3-D image spectrum

Fig. 16 gives an example of these temporal sequences of radar raw-data sub images. In the figure, the spatial structure of the wave field and its time dependence is already visible. Therefore, the three-dimensional image power spectrum $F^3(k, \omega)$ is computed. There are three main contributions to the total spectral energy in the function $F^3(k, \omega)$:

1. Wave energy due to the modulation of the backscatter.

2. Background noise due to the roughness of the sea surface.

3. Higher harmonics of the wave energy due to radar imaging effects.

.

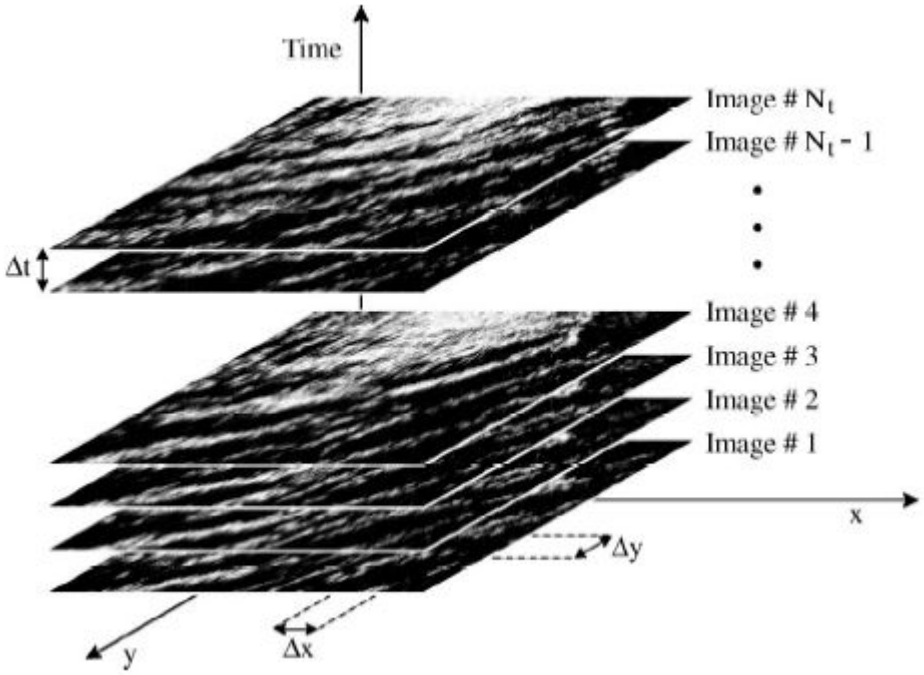

Fig.16 Time series of radar raw data

It is necessary to filter out all the effects that do not belong directly to the wave field, such as the background noise and the higher harmonics. Taking into account Eq 4-4, the wave energy in the three-dimensional image spectrum $F^3(k,\omega)$ must be located in the vicinity of the dispersion shell and can be separated from the

other spectral contributions. The wave energy distribution in the (k,ω) space is strongly dependent on the current U . Fig.17 illustrates the effect of an existing surface current on the wave energy distribution. The example is a projection of a three-dimensional spectrum $F^3(k,\omega)$ to the two-dimensional plane. The black line (a) indicates the dispersion relation without current, the grey line (b) shows how this curve is distorted and the wave energy is shifted due to an existing surface current U .

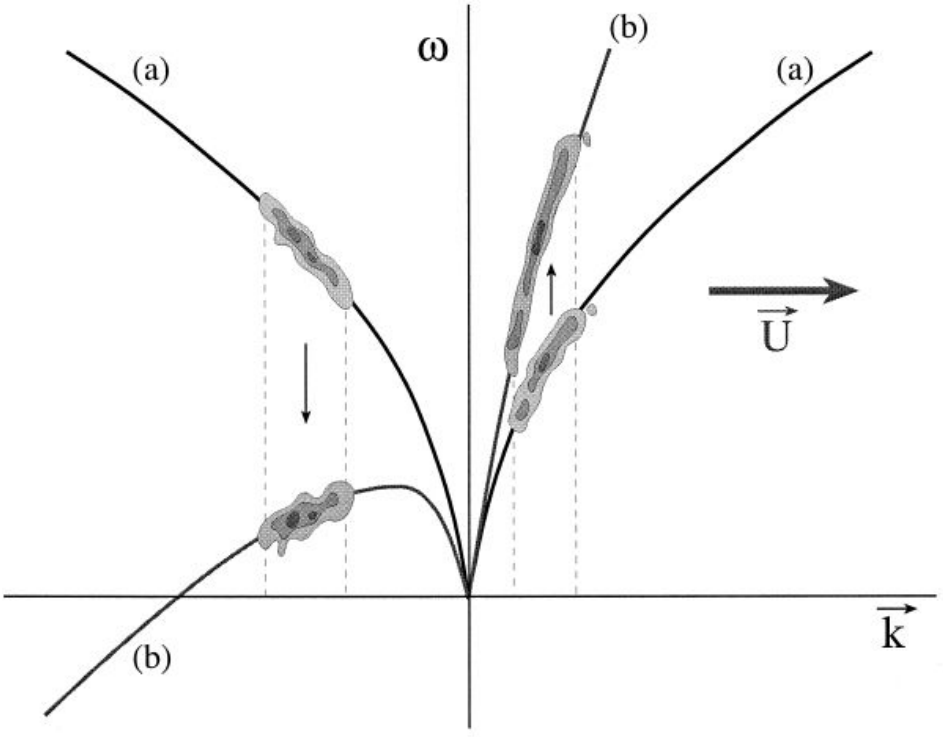

Fig.17. Two-dimensional example of the wave number frequency dependence on the dispersion relation. The line (a) represents the dispersion relation without current, the line (b) shows the shift due to an existing surface current U. The current direction is aligned with the positive wave number.[36]

$$F_f^{(3)}(k_{xn},k_{ym},\omega_p)=$$

$$\begin{cases} F^{(3)}(k_{xn},k_{ym},\omega_p) & \text{if} \\ \qquad \left|\vec{k}(\omega_{p-1},d,\vec{U})\right| \le \left|\vec{k}=(k_{xn},k_{ym})\right| \le \left|\vec{k}(\omega_{p+1},d,\vec{U})\right| & (4.9) \\ 0 & \text{otherwise} \end{cases}$$

where $F_f^{(3)}(k_{xn},k_{ym},\omega_p)$ is the filtered three dimensional image spectrum. Fig.18 shows the original simulated surface elevation and the surface elevation with color Gaussian noise.

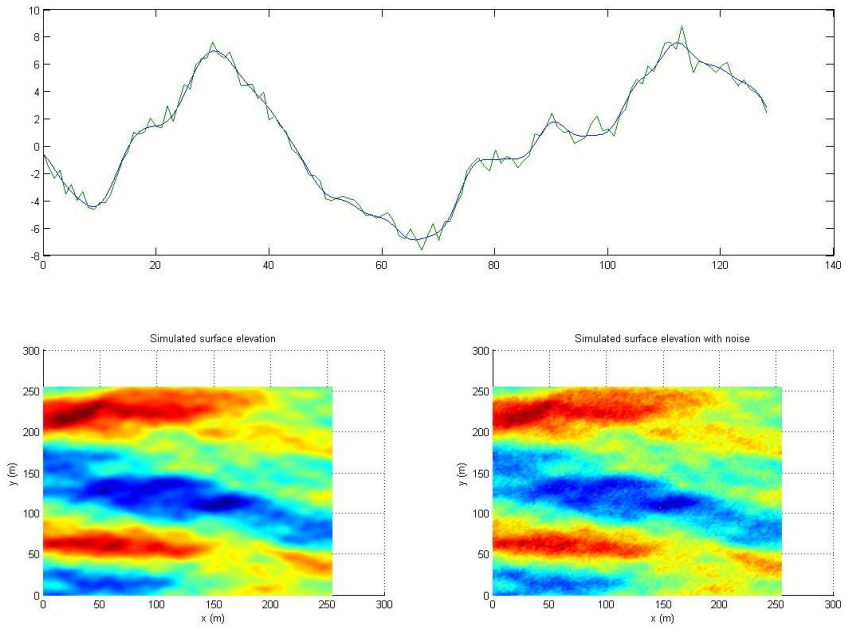

Fig. 18 Original simulated surface elevation and the surface elevation with color Gaussian noise.

4.3.5 Determination of the 2-D image spectrum

In order to obtain the unambiguous directional spectrum three-dimensional spectrum is integrated over the positive frequency domain only:

$$F_f^{(2)}(k_x, k_y) = 2\int_0^{\omega_c} F_f^{(3)}(k_x, k_y, \omega) d\omega \tag{4.10}$$

4.3.6 Determination of the 2-D wave spectrum

4.3.6.1 2-D wave spectrum

To correct the effects of shadowing and tilt modulation on the wave imaging, the filtered two-dimensional image spectrum $F_f^{(2)}(k_x, k_y)$ is transformed into a wave spectrum $E^{(2)}(k_x, k_y)$ by applying a Modulation Transfer Function MTF:

$$E^{(2)}(k_x, k_y) = MTF(k) \cdot F_f^{(2)}(k_x, k_y) \tag{4.11}$$

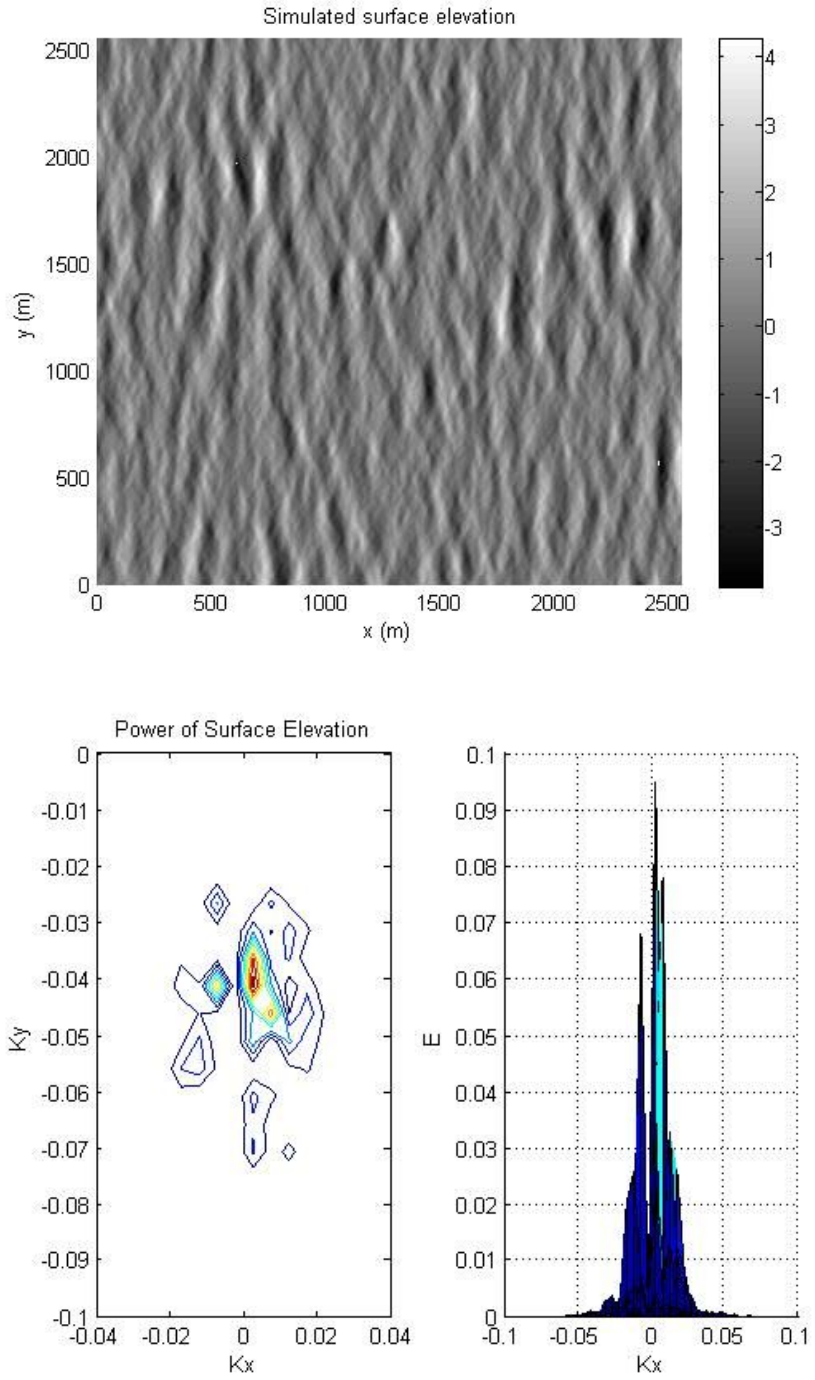

Fig.20 wave spectrum $E(k_x, k_y)$

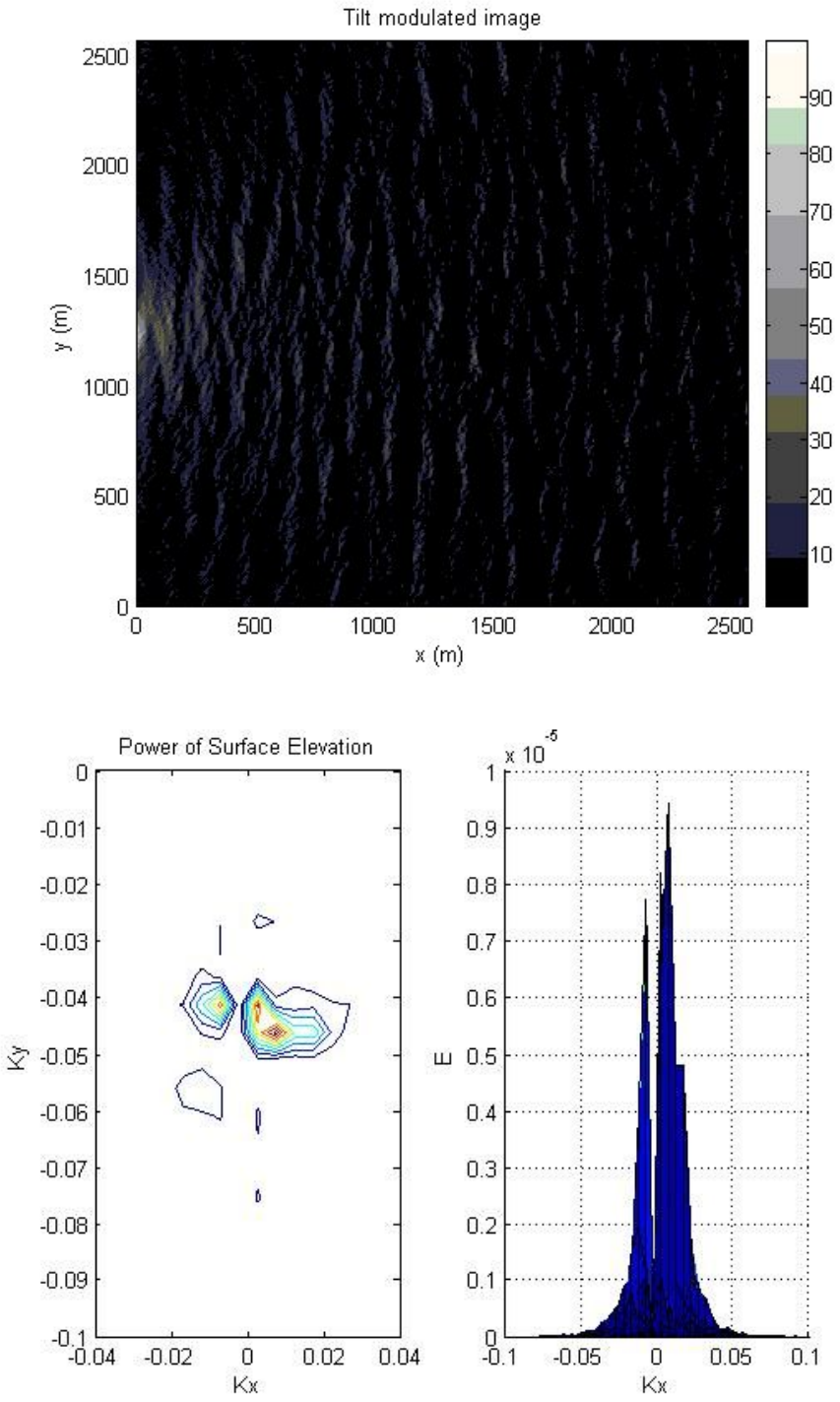

Fig.21 image spectrum

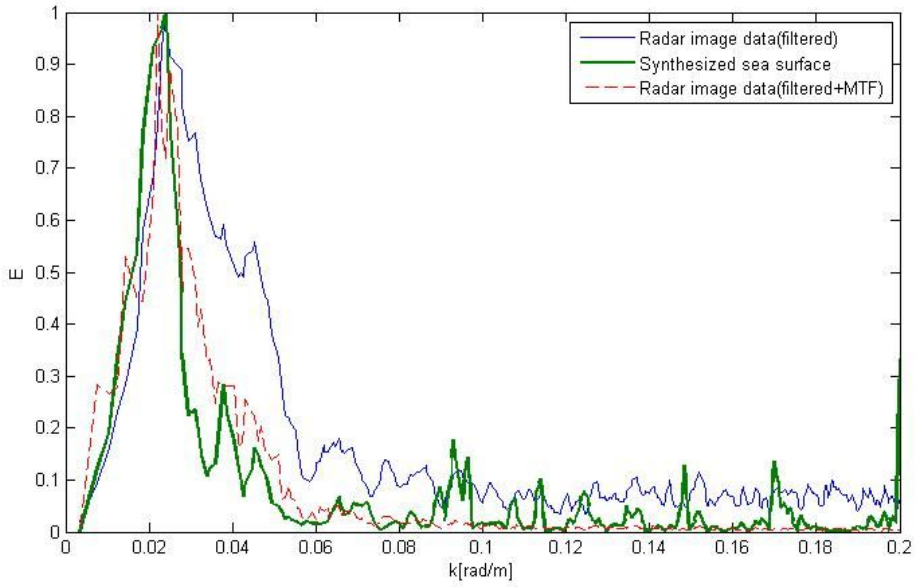

Fig.22 the comparison of wave spectrum obtained by different methods

4.3.6.2 Modulation Transfer Function (MTF)

For horizontal polarization and at grazing incidence, a difference between the image spectra from marine radar imagery and the corresponding spectra from in situ sensors can be observed. This difference is due to the radar wave imaging mechanisms like, for example, shadowing and/or tilt modulation. By using an MTF, this difference can be minimized. In practice, an empirically derived MTF is used, for instance by calibration of measured radar spectra to buoy measurement. The empirical modulation transfer function can be defined as:

$$\left|M(k)\right|^2 = F_r(k) / E_m(k) = k^{\beta} \tag{4.12}$$

where F_r is the radar wavenumber spectrum and E_m is an in-situ measurement (e.g. a with a buoy) or a model spectrum. In the literature, a power decay law for the transfer function has been reported, $\left|M(k)\right|^2 \propto k^{\beta}$, giving a mean value of the exponent β is an empirical coefficient depending on imaging mechanism of the sea surface. In most of the cases presenting a mean value $\overline{\beta}$ =1.21. See table 4

As we discussed before, we already simulated one sea surface, from that sea surface we can get the wave spectrum $E_r^2(k_x, k_y)$ directly. And from the image after adding the shadowing and tilting modulation, we got the image spectrum $F(k_x, k_y)$. From the equation (4-11), we can see,

$$M(k) = F_r(k) / E_m(k) \tag{4.13}$$

And we can get the value of β from minimized following equation:

$$\left|k^{\beta} - F_r(k) / E_m(k)\right| = 0 \tag{4.14}$$

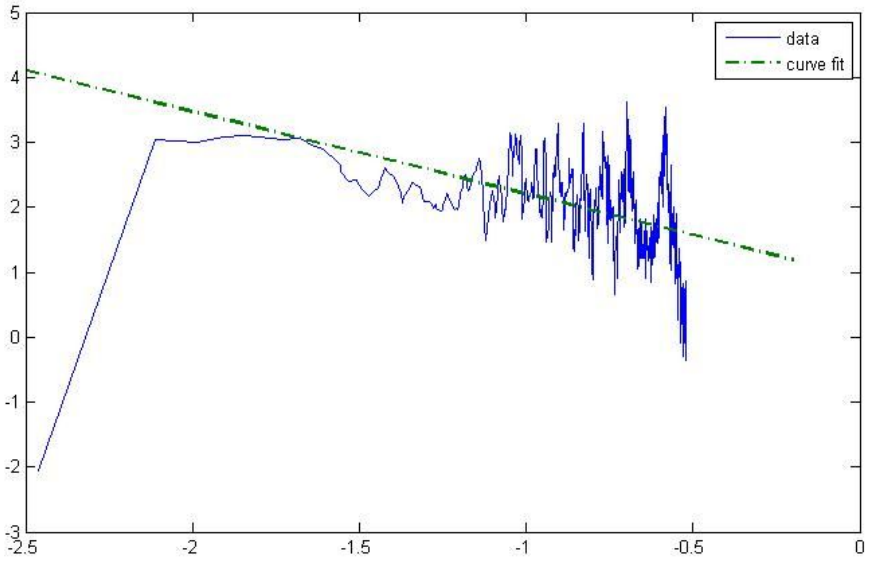

Fig.23 The fit of the MTF exponent β

Table 4. Mean values and variance of the β exponent derived from numerical simulations

Sea state	Modulation	Mean	Variance
Swell	Shadowing	1.22	0.0276
	Shadowing + tilt	1.27	0.0317
Wind sea	Shadowing	1.19	0.0057
	Shadowing + tilt	1.22	0.0078

4.3.7 Computation of the directional wave spectrum:

Once the wave number spectrum $E(\vec{k})$ is computed, other different spectral parameterizations are derived. The most used spectral density is the frequency-direction spectrum. That is defined as:

$$E(\omega,\theta) = E(\vec{k})\frac{dk}{d\omega} \tag{4.15}$$

The expression has been obtained taking into account the dispersion relation. The frequency-direction $E(\omega,\theta)$ leads to the most common sea state parameters, such as peak period, main direction, etc.

4.3.8 Calculation of significant wave height

Due to the non-linearity of the imaging mechanism of ocean waves, the significant wave height can not be determined directly from radar images. However a method to infer wave heights from synthetic aperture radar (SAR) images was developed by and successfully applied [34]. The basic idea of this method is to relate the measured signal-to-noise ratio (SNR) linearly with the significant wave

height of the observed wave field. Applying this relation to WaMoS II data, Hs is given by:

$$H_s = A + B\sqrt{SNR} \tag{4.16}$$

Where A and B are calibration constants which depend on each radar installations and each antenna impulse response. Theses calibration constants are determined within a calibration period by means of a least squares method. The SNR proposed by Alpers and Hasselmann relates the SAR image spectrum with the sum of the clutter and thermal noise spectra. In contrast to this for WaMos II purposes the SNR is defined as:

$$SNR = \frac{SIG}{BGN} \tag{4.17}$$

Where SIG is the energy of the wave spectrum

BGN is the background noise.

For SIG as well as for BGN different definitions have been used. The maximum correlation between the Hs, inferred by WaMoS II and by a buoy has been found for deep water conditions for the following definitions for SIG and BGN:

$$SIG = \sum_{i_x=1}^{N_{kx}} \sum_{i_y=1}^{N_{ky}} E^{(2)}(i_x, i_y) \Delta k_x(i_x) \Delta k_y(i_y) \tag{4.18}$$

$$BGN = \sum_{i_x=1}^{N_{kx}} \sum_{i_y=1}^{N_{ky}} \sum_{i_f=1}^{N_{kf}} F^{(3)}(i_x, i_y, i_f) \Delta f(i_f) \Delta k_y(i_x) \Delta k_x(i_y) - \sum_{i_x=1}^{N_{kx}} \sum_{i_y=1}^{N_{ky}} F^{(2)}(i_x, i_y) \Delta k_y(i_x) \Delta k_x(i_y) \tag{4.19}$$

Where $E^{(2)}$ is the 2-D wave number spectrum and $F^{(3)}$ the 3-D and $F^{(2)}$ the 2-D image spectrum. The extension of the spectra is N_{kx}, N_{ky} and N_{kf} and Δk_x, Δk_y its wave number resolution and Δf its frequency resolution.

4.4 Simulation result

The calibration was performed with a set of 21 signals to noise ratio SNR versus the significant wave height Hs. The parameters of the calibration were calculated by least-square fit of the estimations, which is shown in Fig.22. After the calibration period, the real values of the ocean wave spectra can be estimated from

these and the wave parameters that characterize the sea state. Fig.23 shows the Hs estimated from synthetic radar data.

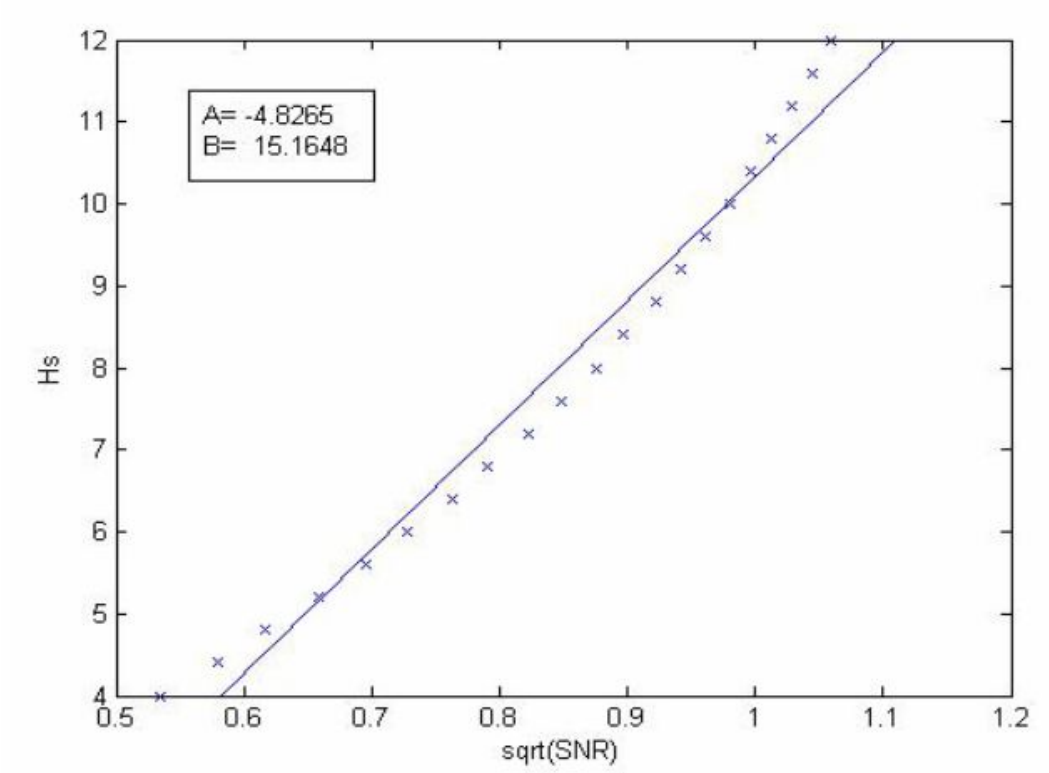

Fig. 24 Scatter plot of the significant wave height and SNR.

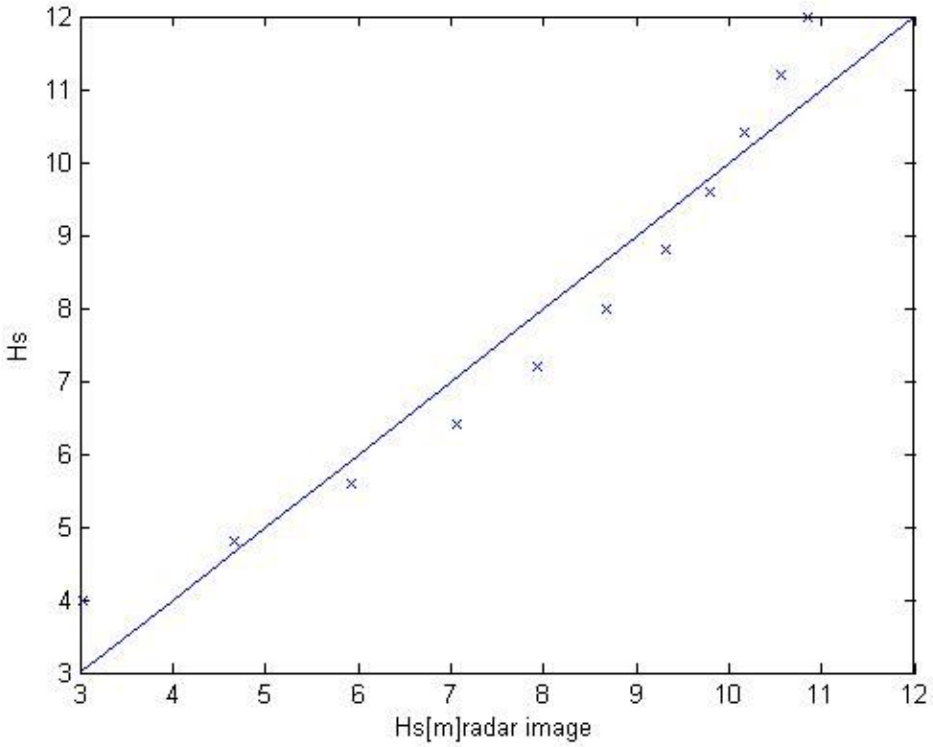

Fig.25 Scatter plot of the significant wave height(Hs)

V. Conclusions

In the present work, the measurement of ocean waves and surface currents with a nautical radar based on the spatial and temporal structure analysis of radar images of the sea surface is presented. This work mainly consists of methods for measuring sea surface states, X-band radar system, inversion of marine radar images and estimation of significant wave height.

Firstly, the comparison among different wave measuring devices such as, buoy and radar methods was summarized; especially the X-band nautical radar and WaMoS II system were introduced in detail.

For estimating sea surface elevation maps from sea clutter images acquired by marine radar, an inversion method was used. This method represents an extension of an existing technique to estimate wave spectra from temporal sequences of marine radar images. It is based on the linear wave theory and assumes the wave field homogeneous in space and stationary in time. To develop this inversion technique, an investigation was carried out to determine empirically the modulation transfer function (MTF) for marine radar measurements (grazing incidence and horizontal polarization), where the MTF exponent β presents a mean value of

1.266. To obtain additional information about the main imaging mechanisms responsible of the radar imagery, various numerical simulations of swell and wind sea were carried out. For each sea state simulation, the respective radar image was determined by considering shadowing only and shadowing plus tilt modulation.

In order to obtain the significant wave height from sequences of nautical radar images, a software was developed. In order to verify the adequacy of the program developed, synthesized images of sea surfaces including shadowing, tilt modulation and Gaussian noise have been created and analysized to estimate the significant wave height. This method based on a technique developed for the determination of significant wave height information from synthetic aperture radar imagery. By analyzing a series of radar images, the calibration was performed with signal to noise ratio SNR versus the significant wave height Hs. The parameters of the calibration were calculated by least-square fit of the estimations (A= -4.8265 , B= 15.1648). Based on this equation, the real values of the ocean wave spectra and the wave parameters that characterize the sea state can be accurately estimated.

VI. Reference

1. Krogstad, H.E., S.F. Barstow, O. Haug, P.O. Marknussen,G. Ueland, and I. Rodriguez (1998). “SMART-800: Remotely Sensed Wave Spectra from a moored buoy”, Proceed. Oceanology’98, Brighton

2. Hasselmann, K. and Hasselmann, S. (1991). “On the nonlinear mapping of an ocean wave spectrum into a synthetic aperture radar image spectrum”. J. Geophys. Res., 96, 10713-10729

3. Ziemer, F. (1995). “An instrument for the survey of the directionality of theocean wave field”. In Proc. of the WMO/IOC Workshop in Oper. Ocean Mon. Using Surface Based Radars, volume 32(99.81-87). Geneva, Swiss

4. Reichert, K., Nieto-Borge, J., and Dittmer, J. (1998). “WaMoS II: Anoperationalwave monitoring system”. In Proc. Oceanology Int. Brighton, U.K.

5. Senet, C., Seemann, J., ans Ziemer, F. (2001). “The near surface current velocity determined from image sequences of the sea surface”. IEEE Trans. Geosci. Remote Sens., 39, 492-505.

6. Outzen, O. (1998). “Bestimmung der Wassertiefe und der oberflachennahen Stromung mit einem nautischen Radar“. In Diploma Thesis, GKSS Report 98/E/60 (inGerman) University of Hamburg, Germany.

7 Hatten, H., Seemann, J., Horstmann, J., Senet, C., and Ziemer, F. (submitted 2003). “Azimuthal and range dependency of sea-surface radar backscatter at

hh-olarization and low grazing incidengce”. IEEE Trans. Geosci. Remote Sens.

8. Ziemer, F. and H. Gunther (1994). “A system to monitor ocean wave fields”. Proceedings of the Second International Conference on Air-Sea Interaction and Meteorology and Oceanography of the Coastal Zone, Lisbon, Portugal.

9. Nieto, J. C., K. Reichert, J. Dittmer, and W. Rosenthal, (1998b). “WaMoS II: A wave and current monitoring system“. Proceed. Of the COST 714 conference on directional wave spectra, Paris, 1998 in press.

10. Nieto, J. C., K. Reichert, J. Dittmer, (1998a): Use of Nautical Radar as a Wave Monitoring Instrument, Submitted for publication in Coastal Engineering, 1998.
11. Alpers, W., and K. Hasselmann, (1982): Spectral Signal to Clutter and Thermal Noise Properties of Ocean Wave Imaging Synthetic Aperture Radars. Int. J. Rem. Sens., 3, pp 423-446.

12 Croney, J. (1970): Radar handbook: civil marine radar. Merril I. Skolnik.

13 Nieto, J.C. (1997): Analisis de campos de oleaje Mediante Radar de Navegacion en Banda, Ph.D. thesis at the dep. Of physics of the University of Madrid.

14 Lee, P.H. Y., and Coauthors, (1995): X-Band microwave backscattering from ocean waves. J. Geophys. Res., 100, 2591-2611.

15 Plant, W. J., and W. C. Keller, (1990): Evidence of Bragg scattering in microwave Doppler spectra of sea return. J. Geophys. Res., 95, 16 299- 16 310

16 Wenzel, L. B., (1990): Electromagnetic scattering from the sea at low grazing angles. Surface Waves and Fluxes, G. L. Geernaert and W. J. Plant, Eds., Kluwer Academic, 41-108.

17 Young, I. R., Rosenthal, and F. Ziemer, (1985): Three-dimensional analysis of marine radar images for the determination of ocean wave directionality and surface currents. J. Geophys. Res., 90, 1049-1059.

18 Ziemer, F., and W. Rosenthal, (1991)Directional spectra from ship-board navigation radar during LEWEX. Directional Ocean Wave Spectra: Measuring, Modeling, Predicting, and Applying, R. C. Beal, Ed., The Johns Hopkins University Press, 125-127

19 Nieto Borge, and C. Guedes Soares, (2000): Analysis of directional wave fields using X-Band navigation radar. Coastal Eng., 40, 375-391

20 Hessner, K., K. Reichert, J. C. Nieto Borge, and H. Gunther, (2001): Evaluation of WaMos II wave data. Proc. Fourth Int. Symp. On Ocean Wave Measurement and Analysis, San Francisco, CA, ASCE, 221-230

21 Mitsuyasu, H., F. Tasai, T. Suhara, S. Mizuno, M. Ohkusu, T. Honda, and K. Rikiishi, (1980): Observation of the power spectrum of ocean waves using a coverleaf buoy. J. Phys. Oceanogr., 10, 286-296

22 Plant, W. J., and L. M. Zurk, (1997): Dominant wave directions and significant wave heights from SAR imagery of the ocean. J. Geophys. Res., 3473-3482

23 Seemann, J., F. Ziemer, and C. M. Senet, (1997): A method for computing calibrated ocean wave spectra from measurements with a nautical X-Band radar. Proc. Conf. on 500 years of Ocean Explorations, Halifax, NS, Canada, IEEE, 1148-1154

24 Valenzuela, G.R., (1978): Teories for the interaction of electro-magnetic and oceanic waves a review. Boundary-Layer Meteorology, 13, pp87-105

25 Alpers, W, D.B. Ross, and C.L. Rufenach, (1981): On the detectability of ocean surface waves by real and synthetic aperture radar. J. Geophys. Res., 86, pp 6481-6498

26 Plant, W. J., (1990): Bragg Scattering of Electromagnetic Waves from Air/Sea Interface. Surface Waves and Fluxes, II, Kluwer Academic Publishers. Printed in the Netherlands, PP 41-108

27 Wetzel, L.B., (1990): Electromagnetic Scattering from the Sea at Low Grazing Angles. Surface Waves and Fluxes, II, pp 41-108, Kluwer Academic Publishers. Printed in the Netherlands.

28 Ziemer F. and W. Rosenthal, (1987): on the Transfer Function of a Shipborne Radar for imaging ocean waves. Proc. IGARSS'87 Symp. Ann Arbor. Michigan, May 1987, pp 1559-1564

29 Dittmer, J., (1995): Use of marine Radars for Real Time Wave Field Survey and Speeding up the Transmission/Processing. Proceed. Of the WMO/IOC Workshop on Operational Ocean Monitoring using Surface Based Radars, Geneva, March (1995)

30 Ziemer F. (1991): Directional Spectra from shipboard Navigation Radar during LEWEX. Directional Ocean Wave Spectra, Edited by Robert C. Beal, The John Hopkins University Press.

31 Senet, C.M., J. Seemann, and F. Ziemer (1997): An Interactive Technique to Determine the Near Surface Current Velocity From Time series of Sea surface Images. Proc. OCEANS'97, 500years Ocean Explorations, Halifax, Canada, October 1997.
32 Atanassov, V., W. R$osenthal, and F. Ziemer, (1985): Removal of Ambiguity of Two dimensional Power Spectra Obtained by Processing Ship Radar images of Ocean waves. J. Geophys. Res., 90, pp 1061-1067.

33 R. H. Stewart and J. W. Joy, "HF radio measurements of surface currents,"Deep Sea Res., vol. 21, pp. 1039–1049, 1974.

34 Bruning, C., S. Hasselmann, K. Hasselmann, S. Lehner, and T. Gerling, (1994): First evaluation of ERS-1 synthetic aperture radar wave mode data. Global Atmosphere and Ocean Systems, 2, 61-98.